Numerical Simulation of Direct Detonation Initiation in $H_2/O_2/Ar$ Mixtures with Detailed Chemistry

Chengken Qi, Zheng Chen
SKLTCS, Department of Mechanics and Engineering Science, College of Engineering,
Peking University, Beijing 100871, China

1 Introduction

During direct detonation initiation, detonation is instantaneously formed by the driven blast wave as a result of a large amount of energy deposited in a gaseous explosive mixture. According to He and Clavin [1], there are three regimes of direct detonation initiation, namely supercritical, critical and subcritical, based on the ratio between deposited energy and the critical energy E_C. In the supercritical regime, the deposited energy is much larger than E_C. The overdriven detonation decays and asymptotically approaches to the self-sustained CJ detonation. In the critical regime, the deposited energy is slightly larger than E_C. The shock wave first decays and the reaction front decouples from it, until a quasi-steady period, during which the shock speed and reaction front speed remain constant [2]. At the end of the quasi-steady period, local explosion induced pressure pulse accumulates quickly and accelerates the reaction front speed and the shock speed. Finally a detonation is formed [2]. In the subcritical regime, the deposited energy is lower than E_C. The shock wave speed always decreases and the reaction front decouples from the shock, which leads to detonation initiation failure. Zeldovich et al. [3] first proposed a qualitative criterion relating the critical energy E_C and the induction length (or induction time).

Recently, many attempts have been focused on predicting the critical energy under various initial conditions. For examples, He and Clavin [1,4] proposed the critical curvature model (DR model, D is detonation speed, and R is radial location) to predict the critical condition of direct detonation initiation based on their quasi-steady analysis neglecting the unsteady effect; Eckett et al. [5] found that the dominant failure mechanism is the unsteady effect rather than curvature effect, based on which they proposed the critical decay rate model; and Kasimov et al. [6,7] established the $\dot{D} - D - \kappa$ model ($\dot{D}$ is detonation acceleration, D is detonation speed, and κ is the curvature), in which curvature and unsteadiness are both considered. A review has been conducted by Zhang and Bai very recently [8]. However most previous theories were based on one-step reaction model, for which the critical energy in fact does not exists since detonation can be always initiated if there is enough time for reaction (no matter how large the initiation energy is) [9]. Lee and Higgins [10] suggested that the single-step reaction model should be abandoned, and multi-step reaction model should be used. Short et al. [11] and Ng et al. [2] employed a three-step reaction model in their simulation of direct detonation initiation, and found that detonation initiation fails when the blast wave temperature decays below the chain-branching cross-over temperature before detonation is formed.

There are only a few studies on direct detonation initiation considering detailed chemistry. He et al. [4] first employed detailed reaction mechanism to simulate direct detonation initiation for $H_2/O_2/Ar$ mixtures, however, few details were demonstrated. Im et al. [12] and Wang et al. [13] used detailed

Correspondence to: cz@pku.edu.cn

reaction mechanism for $H_2/O_2/Ar$ mixtures to study the direct detonation initiation. However, the quasi-steady and detonation development processes for critical regime were still not well understood. The object of this study is to analyze different processes involved in direct detonation initiation considering detailed chemistry. One-dimensional simulations for direct detonation initiation in $H_2/O_2/Ar$ mixtures are conducted. In the following, the numerical model is introduced in Section 2; and the results and discussion are presented in Section 3; and finally the conclusions are summarized in Section 4.

2 Numerical model

Direct initiation of a cylindrical detonation in $H_2/O_2/Ar$ (molar ratio 2:1:7) mixtures initially at 0.2 atm and 298 K is simulated using the in-house code A-SURF [14-16]. A-SURF solves the conservation equations for one-dimensional, compressible, multi-component, reactive flow using the finite volume method. Detailed hydrogen mechanism developed by Conaire et al. [17] is employed in simulation. Dynamically adaptive mesh refinement strategy is adopted, so that the reaction front, shock wave and detonation are efficiently resolved. The details of this code concerning governing equations, numerical methods, and code validation can be found in Refs. [14-16].

In order to initiate the detonation, the ideal strong blast wave model is adopted as the initial condition. The same approach was used in previous studies (e.g., [2,5,9]). The computational domain is $0 \leqslant r \leqslant 80$ cm. Zero flow speed and zero gradients of temperature and mass fractions are enforced at the center (r=0) and right boundary (r=80 cm). The finest mesh size is 2 μm and the corresponding time step is 0.1 ns since explicit integration method is used.

3 Results and Discussion

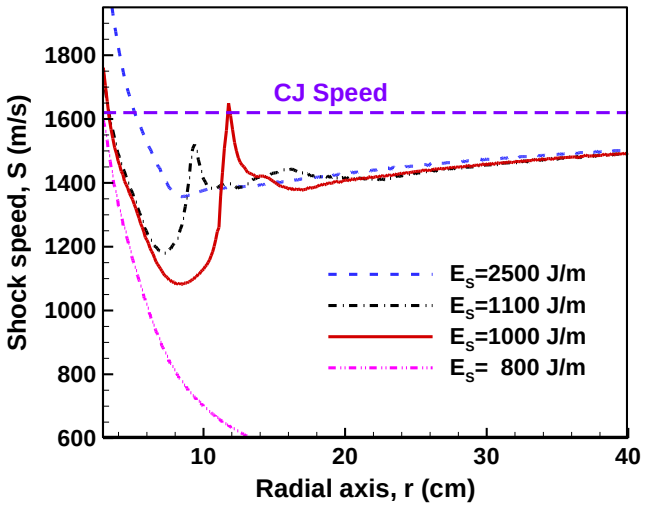

Fig. 1. The shock speeds as a function of radial location of cylindrical detonation initiation at different initial energies (H_2:O_2:Ar = 2:1:7 initial condition of P_0=0.2 atm, T_0=298 K).

Figure 1 shows the evolution of shock speeds at different initiation energies. For reference, the CJ speed is also plotted. The initial energy of E_S=800 J/m corresponds to the subcritical regime, in which detonation initiation fails. The strong blast wave is shown to decay all the time and finally decay to a compression wave propagating at the sound speed. In the critical regime with E_S=1000 or 1200 J/m, the blast wave is shown to first decay to a speed below 75% of CJ speed. After experiencing a short period of nearly constant speed, (which is called "quasi-steady" regime), it reaccelerates abruptly to form an overdriven detonation. After that, it decays again and asymptotically approaches to the CJ speed. In the supercritical regime with E_S=2500 J/m, the blast wave decays to some value below CJ speed and then slowly accelerates. It is noted that even for the supercritical case, the lowest value of

shock speed is less than CJ value. This is because the cylindrical rather than planar geometry is considered here [18].

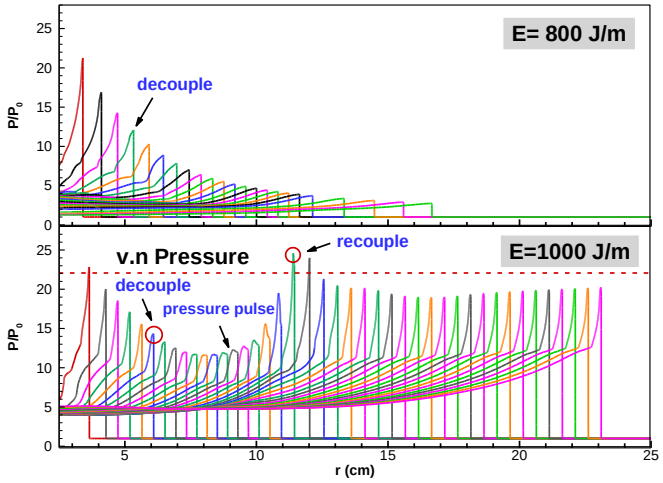

Fig. 2. Distribution of normalized pressure at different times for the subcritical (E_S=800 J/m) and critical (E_S=1000 J/m) cases.

Figure 2 shows the temporal evolution of pressure distributions for subcritical and critical cases. For the subcritical case with E_S=800 J/m, reaction front starts to be decoupled from the shock wave when it reaches around r=5.2 cm, after which the distance between them increases (see Fig. 3). At the same time, the maximum pressure behind the shock wave decreases. Consequently, detonation initiation fails. For the critical case with E_S=1000 J/m, the reaction zone starts to decouple with the shock wave when it reaches about r=6.2 cm. It is observed that there exists a period of quasi-steady state, during which the peak pressure and the distance between reaction front and shock wave remain unchanged. At the end of this quasi-steady process, reaction-generated pressure pulse arises and it propagates towards the shock. The coherent coupling of pressure pulse with heat release eventually results in the coupling between the reaction zone and leading shock wave, which can be explained by the Shock Wave Amplification by Coherent Energy Release (SWACER) mechanism of Lee [19].

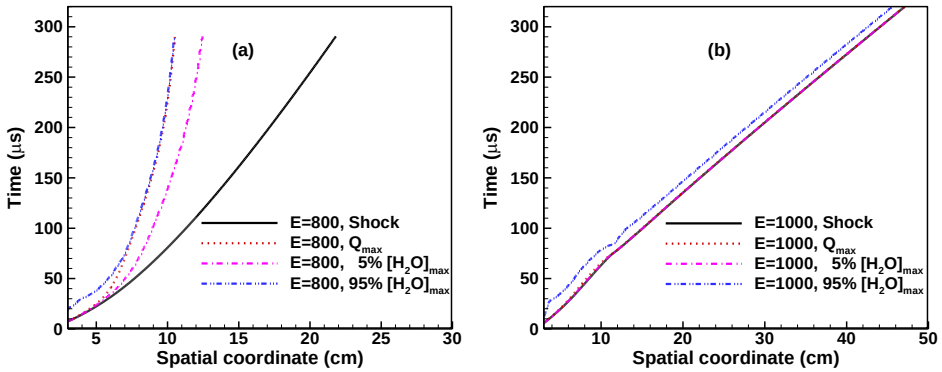

Fig. 3. Evolution of the location of shock wave and reaction zone of direct detonation initiation with (a) E_S=800 J/m, (b) E_S=1000 J/m.

Since the mass fraction of H_2O varies from 0 to maximum value $[H_2O]_{max}$ in the reaction zone, 5% and 95% of $[H_2O]_{max}$ can be used to indicate the width of the reaction zone. The results for the subcritical and critical cases are plotted in Fig. 3, in which the position of maximum total heat release rate, Q_{max}, is also shown. For the subcritical case with E_S=800 J/m, the reaction zone starts to decouple from the shock at r=5.2 cm. For the critical case with E_S =1000 J/m, the reaction zone is shown to be always coupled with shock wave, except when it is between r=6.2 cm and r=11.0 cm.

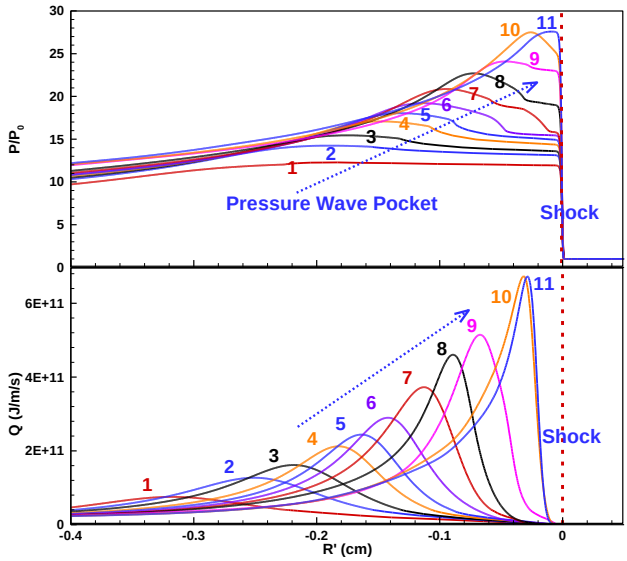

Fig. 4. Pressure and heat release rate profiles at different times during the re-acceleration process with initiation energy of E_S=1000 J/m. In the shock-reference-frame, we have R'=r-R_S, where R_S=R_S(t) is the position of shock wave. The time sequence is 1, t=56.78 μ s; 2, t=65.75 μ s; 3, t=67.56 μ s; 4, t=69.36 μ s; 5, t=70.26 μ s; 6, t=71.16 μ s; 7, t=72.07 μ s; 8, t=72.97 μ s; 9, t=74.77 μ s; 10, t=75.68 μ s; 11, t=76.22 μ s.

In the following we focus on the quasi-steady period and the mechanism of pressure pulse amplification. Figure 4 depicts the process during which heat release and pressure pulse propagation are coupled and pressure pulse is amplified in the shock-reference frame. Line #1 corresponds to results in the quasi-steady period. After the shock, there is an induction zone after which reaction zone appears. At the end of induction zone, the mixture is in the state close to auto-ignition. When local auto-ignition occurs, a small pressure pulse is generated as indicated by line #2. This pressure pulse propagates towards the leading shock wave. At the beginning, this pressure pulse is not strong enough and thereby the mixture does not auto-ignite immediately when it is passed by the pressure pulse. However, the subsequent auto-ignition further produces pressure pulse propagating at higher speed than the original one. Consequently, the pressure pulse accumulates and becomes stronger. The stronger pressure pulse then results in faster auto-ignition. Therefore, the pressure pulse is coherently coupled with heat release (lines #4~#11). Lines #1 to #11 indicate that the reaction zone is always inside the pressure wave pocket and it eventually is synchronized with the pressure pulse wave propagation. In this way, an overdriven detonation is formed as in the SWACER mechanism.

The particle tracking method is used here to analyze the detonation initiation process. The heat release rates of different particles in the shock-reference frame are shown in Fig. 5. From particle #1 to #8, shock strength decays rapidly during the blast energy dominated propagation process. It is observed that the heat release rate decreases and reaction zone moves away from the shock. A transition of the trend is observed for particles #9 to #14. Because of the coherent coupling between pressure pulse and local auto-ignition, the peak of particle heat release rate increases, and the reaction zone moves quickly close to the shock. Figure 6 shows the p-v diagrams for different particles. The particles in Fig. 6(a) experience the late stage of the quasi-steady period and the early stage of the re-acceleration process. Point A corresponds to the initial undisturbed states, and point B corresponds to states right after the shock wave. Curve AB is the Hugoniot curve. As the shock strengthens, point B of following particles moves up. In Fig. 6(b), the post-shock state of the particle at r=11.6 cm has the highest pressure (see point C), which denotes an over-driven detonation. After that, it decays and point B moves downside. After the shock, the particle at r=8.1 cm experiences nearly constant-pressure combustion. On the other

hand, the particle at r=10.0 cm experiences nearly constant-volume combustion. The particles between these two experience neither constant-pressure nor constant-volume combustion.

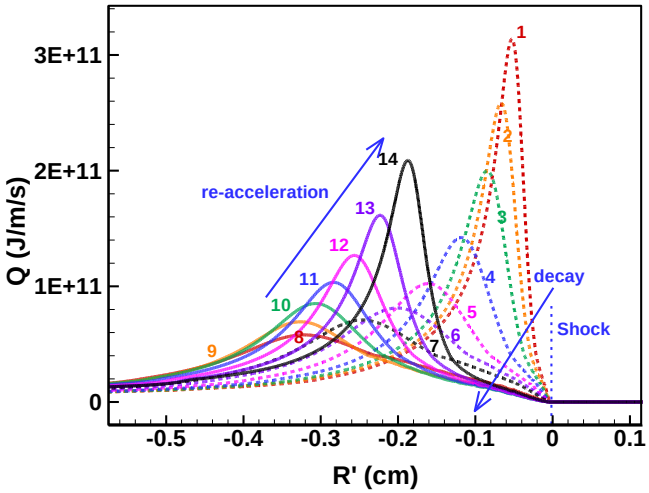

Fig. 5. Heat release rate of different particles. E_S=1000 J/m. The initial location of each particle is: 1, r=4.1 cm; 2, r=4.6 cm; 3, r=5.0 cm; 4, r=5.4 cm; 5, r=5.8 cm; 6, r=6.0 cm; 7, r=6.4 cm; 8, r=7.0 cm; 9, r=7.9 cm; 10, r=8.8 cm; 11, r=9.2 cm; 12, r=9.5 cm; 13, r=9.8 cm; 14, r=10 cm.

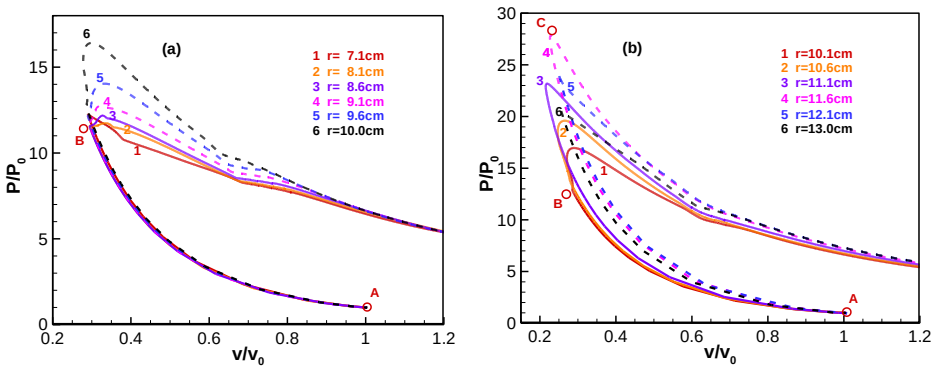

Fig. 6. P-v (pressure-specific volume) diagrams for different particles. E_S=1000 J/m.

4 Conclusions

Direct initiation of cylindrical detonation is simulated with detailed chemistry for hydrogen. The initiation model of ideal strong blast wave model is used. The emphasis is on the quasi-steady state and re-acceleration process in the critical regime. During the quasi-steady period, the shock speed and post-shock pressure remain nearly constant. However, the pressure pulse arises and accumulates until fast amplification occurs. Shock-reference-frame is used to demonstrate the coupling between the pressure pulse and heat release at the re-acceleration stage. Particle tracking method is used to show particle heat release rates and particle pressure-specific volume plane, which helps to distinguish different stages of evolution of direct detonation initiation.

Acknowledgements

This work was supported by National Natural Science Foundation of China (Nos. 51322602 and 51136005) and State Key Laboratory of Engines at Tianjin University (No. K2014-01).

References:

[1] He L. & Clavin P. (1994). On the direct initiation of gaseous detonations by an energy source. Journal of Fluid Mechanics. 277:227-248.

[2] Ng H.D. & Lee J.H.S. (2003). Direct initiation of detonation with a multi-step reaction scheme. Journal of Fluid Mechanics. 476:179-211.

[3] Zeldovich I.B. et al. (1956). An experimental investigation of spherical detonation of gases. Soviet Physics-Technical Physics. 1:1689-1713.

[4] He L. (1996). Theoretical determination of the critical conditions for the direct initiation of detonations in hydrogen-oxygen mixtures. Combustion and Flame. 104:401 - 418.

[5] Eckett C.A. et al. (2000). The role of unsteadiness in direct initiation of gaseous detonations. Journal of Fluid Mechanics. 421:147-183.

[6] Kasimov A.R. & Stewart D.S. (2004). Theory of direct initiation of gaseous detonations and comparison with experiment. Department of Theoretical and Applied Mechanics (UIUC).

[7] Kasimov A.R. (2004). Theory of instability and nonlinear evolution of self-sustained detonation waves. University of Illinois at Urbana-Champaign, Urbana, Illinois.

[8] Zhang B. & Bai C. (2014). Methods to predict the critical energy of direct detonation initiation in gaseous hydrocarbon fuels – An overview. Fuel. 117:294-308.

[9] Mazaheri Body K. (1997). Mechanism of the onset of detonation in blast initiation. McGill University, Montreal.

[10] Lee J.H.S. & Higgins A.J. (1999). Comments on Criteria for Direct Initiation of Detonation. The Royal Society. 357:3503-3521.

[11] Short M. & Quirk J.J. (1997). On the nonlinear stability and detonability limit of a detonation wave for a model three-step chain-branching reaction. Journal of Fluid Mechanics. 339:89-119.

[12] Im K. & Yu S.T. (2003). Analyses of Direct Detonation Initiation with Realistic Finite-Rate Chemistry. 41st AIAA Aerospace Sciences Meeting & Exhibit. Reno, NV.

[13] Wang B. (2010). Numerical Simulation of Detonation Initiation by the Space-Time Conservation Element and Solution Element Method. The Ohio State University, OH.

[14] Chen Z. et al. (2011). On the critical flame radius and minimum ignition energy for spherical flame initiation. Proceedings of the Combustion Institute. 33:1219-1226.

[15] Chen Z. (2010). Effects of radiation and compression on propagating spherical flames of methane/air mixtures near the lean flammability limit. Combustion and Flame. 157:2267-2276.

[16] Chen Z. et al. (2009). Effects of Lewis number and ignition energy on the determination of laminar flame speed using propagating spherical flames. Proceedings of the Combustion Institute. 32:1253-1260.

[17] O Conaire M. et al. (2004). A comprehensive modeling study of hydrogen oxidation. International Journal of chemical kinetics. 36:603-622.

[18] Lee J.H.S. (2008). The detonation phenomenon. Cambridge University Press Cambridge.

[19] Lee J.H.S. et al. (1978). Photochemical initiation of gaseous detonations. Acta Astronautica. 5:971-982.